RESEARCH

Functional analysis of JPH2-knockout cardiomyocytes identifies ECCD as a novel indicator in a human cardiac modelJPH2

Tianwei Guo[1†], Hongyue Wang[1†], Fujian Wu[1†], Wenjing Lu[2], Min Zhu[3], Shuhong Ma[1], Yongshuai Zhang[3], Yuting Yan[1], Meng Zhou[1], Didaer Talanaite[1], Siyu Liu[1], Man Qi[1,3,4,5,6*], Feng Lan[7,8*] and Xujie Liu[9*]

Abstract

Background Junctophilin-2 (JPH2) is a vital protein in cardiomyocytes, anchoring T-tubule and sarcoplasmic reticulum membranes to facilitate excitation-contraction coupling, a process essential for cardiac contractile function. Dysfunction of JPH2 is associated with cardiac disorders such as heart failure; however, prior studies using mouse models or primary human cardiomyocytes are limited by interspecies differences or poor cell viability, respectively. This study aimed to investigate JPH2's role in human cardiac function and disease using a novel stem cell-derived model, while introducing a new indicator to evaluate related cardiac impairments.

Methods We generated a JPH2-knockout model using human embryonic stem cell-derived cardiomyocytes (hESC-CMs) with CRISPR/Cas9. Cellular morphology, contractile function, calcium dynamics, and electrophysiological properties were assessed via transmission electron microscopy, the CardioExcyte96 system, calcium imaging with Fluo-4 AM, and multi-electrode array recordings, respectively. Wild-type JPH2 was overexpressed through lentiviral transfection to evaluate rescue effects, and two JPH2 variants—one benign (G505S) and one pathogenic (E85K)— were introduced to study mutation-specific effects.

Results JPH2 knockout disrupted excitation-contraction coupling in hESC-CMs by impairing junctional membrane complex structure, leading to heart failure-like phenotypes with reduced contractility, altered calcium dynamics, and electrophysiological irregularities. Overexpression of wild-type JPH2 restored these functions, affirming its critical role in cardiac physiology. We identified excitation-contraction coupling delay (ECCD) as a novel indicator that precisely quantified coupling impairment severity, with its applicability validated across distinct JPH2 variants (G505S and E85K).

---

†Tianwei Guo, Hongyue Wang and Fujian contributed equally to this work

*Correspondence:
Man Qi
qimandonkey@163.com
Feng Lan
fenglan@ccmu.edu.cn
Xujie Liu
liuxujie@fuwaisz.cn

Full list of author information is available at the end of the article

Conclusions This study demonstrates JPH2's essential role in sustaining excitation-contraction coupling by stabilizing the junctional membrane complex, with its deficiency driving heart failure-like cardiac dysfunction. ECCD is established as a sensitive, comprehensive indicator for assessing JPH2-related impairment severity. These findings advance our understanding of JPH2 in cardiac pathology and position ECCD as a valuable tool for research and potential clinical evaluation, with JPH2 and calcium regulation emerging as promising therapeutic targets.

Keywords Junctophilin 2, Excitation-contraction coupling, Cardiomyopathy, Human embryonic stem cell-derived cardiomyocytes

Introduction

Cardiovascular diseases are currently the most prevalent diseases threatening global health and life [1–3]. The onset of cardiovascular diseases often stems from the impairment of cardiac contractile function. Contractile function of the heart relies on the contraction and relaxation of the myocardium, with excitation-contraction coupling (ECC) serving as the basis for maintaining contractile function in cardiomyocytes [4, 5]. Any dysfunction in the ECC process can trigger various cardiac diseases.

ECC relies on a complex structural foundation [4]. T-tubules, formed by invaginations of the cardiomyocyte membrane, penetrate deep into the cell and make close contact with the sarcoplasmic reticulum (SR). L-type calcium channels (LTCC) located on the T-tubules allow a small influx of calcium, which activates the ryanodine receptor 2 (RyR2) on the SR membrane, triggering calcium-induced calcium release (CICR). This release of calcium from the SR into the cytoplasm initiates muscle contraction. Crucial to this process is the distance between the T-tubule membrane and the SR membrane. This spatial relationship is maintained by the junctional membrane complex (JMC) [6]. The JMC couples ion channels on these two membranes, ensuring signal transmission for cardiomyocyte contraction. Disruption to the morphology of JMC is closely linked to various cardiac diseases. The formation and stabilization of the JMC are primarily dependent on the JPH2 protein [7, 8]. By tightly anchoring the T-tubules and the SR membranes, JPH2 enables the normal operation of ion channels within the JMC, thus maintaining the ECC process in cardiomyocytes [9, 10].

JPH2 is a member of the junctophilin family, which comprises four subtypes [11–14]. Among them, JPH2 is specifically expressed in the heart. JPH2 protein consists of six structural domains: MORN I region, linker region, MORN II region, α-helix-like region, variable region, and transmembrane region. In mouse models, it has been demonstrated that the N-terminal MORN domain of JPH2 exhibits a high affinity for phospholipids and is capable of binding to the T-tubule/plasma membrane (PM) [7, 15]. The C-terminal transmembrane domain, composed of 20 hydrophobic amino acids, can be inserted into the SR membrane. Through anchoring to these two membranes, JPH2 plays a crucial role in maintaining the structure of the JMC, thereby ensuring the stability of the dyad [16, 17]. Moreover, JPH2 interacts with and exerts regulatory effects on multiple ion-channel proteins within the JMC structure, such as LTCC and RyR2 [18–21].

Considering the critical role that JPH2 plays in maintaining the structure of myocardial JMCs, the loss of JPH2 function can exert a substantial impact on cardiac function [20, 22–26]. Analysis of heart failure (HF) tissue samples has shown a downregulation of JPH2 expression [11, 14, 27, 28]. In Vitro functional studies also suggest that JPH2 mutations may lead to the development of HF. Gene-knockout models are a widely adopted approach for exploring the mechanisms underlying the role of downregulated genes in diseases. In particular, the JPH2-gene-knockout myocardial model can be used to probe the physiological and molecular changes within the myocardium after JPH2 downregulation, thus enabling researchers to elucidate the potential mechanisms by which JPH2 downregulation drives HF progression. Numerous studies have reported mouse models with JPH2 knockout or knockdown [7, 10, 29, 30]. Nevertheless, significant disparities exist between the murine and human hearts in terms of anatomical structure, physiological functions, and gene expression regulation. These differences render it challenging to directly and accurately extrapolate the findings from mouse models to humans, thus limiting their ability to provide precise references for the research and treatment of human heart diseases. Primary human myocardial tissues from HF patients have demonstrated the down-regulation of JPH2 expression. However, cardiomyocytes isolated from the heart exhibit a low survival rate and a short survival time under In Vitro culture conditions. This restricts the feasibility of conducting in-depth and systematic experimental research.

In light of the limitations associated with existing research models, our study aimed to overcome these bottlenecks. We established a human embryonic pluripotent stem cell-derived cardiomyocytes (hESC-CMs) JPH2 knockout model with CRISPR/Cas9. This novel model effectively breaks through the bottleneck of species-related limitations and is amenable to large-scale production and in-Vitro cultivation [31, 32]. Using this model,

we thoroughly explored the critical role of JPH2 in maintaining cardiac physiological activities In Vitro from various aspects, including cell morphology, contractile function, calcium transients, and electrical activities, and also investigated the potential mechanisms underlying the development of heart diseases associated with JPH2 deficiency. Moreover, this study introduces a novel indicator, the excitation-contraction coupling delay (ECCD), for assessing the pathogenicity of JPH2-related diseases.

Methods

Cell culture

H9 hESCs were utilized in this study. Cells were cultured in E8 medium (Cellapy) on Matrigel-coated plates. The cultures were maintained at 37 °C in a 5% CO_2 incubator, and the medium was refreshed daily. When the cell confluence reached 70–80%, the cells were passaged using 0.5 mM EDTA.

Genome editing

We used the epiCRISPR/Cas9 gene-editing system to generate the JPH2-knockout H9 hESC cell line. Details can be found in our previously published work. With the help of online design tools like CRISPOR (http://crispor.tefor.net/), the guide RNA (gRNA) was designed to target exon 2 of the *JPH2* gene. The designed gRNA sequence was synthesized by Synbio Technologies. Then, the gRNA was cloned into the epiCRISPR/Cas9 vector, and the resulting vector was transformed into TOP10 Escherichia coli cells (Thermo Fisher). After growing overnight on LB agar plates with ampicillin (100 μg/mL),

single colonies were selected for plasmid extraction by the EndoFree Maxi Plasmid Kit (TIANGEN BIOTECH). Sanger sequencing verified the correct gRNA sequence insertion.

Approximately 1×10^5 H9 cells were electroporated with 5 μg of the sgRNA vector following the CA137 protocol using the LONZA 4D transfection system (Lonza). The cells were then seeded in a 6-well plate and cultured in E8 medium supplemented with 10 μM Y-27,632. After 24 h, the medium was replaced with E8 medium containing 0.3 μg/mL puromycin. About 10 days after electroporation, puromycin-resistant clones were established. Fifteen clones were picked using a 1 mL sterile syringe and expanded in a 24-well plate. Genomic DNA was extracted from all clones using the TIANamp Genomic DNA Kit (TIANGEN BIOTECH). The primer sequences for *JPH2* are listed in Table 1. Sanger sequencing was carried out by Sino Geno Max to screen for clones with the desired JPH2 genomic modification.

In vitro cardiomyocyte differentiation

Cardiomyocytes were differentiated using a chemically defined molecular-based method. After the cells seeded in a Matrigel-coated 6-well plate at 1:6 ratio achieved around 75% confluence, the differentiation of human cardiomyocytes was initiated with the employment of the CardioEasy® Human Cardiomyocyte Differentiation Kit (Cellapy). Spontaneous contractions were observed from days 7–8 after differentiation. On day 12, the cells were purified using CaridoEasy® Human Cardiomyocyte Purification Medium (Cellapy).

Flow cytometry analysis

Cells were detached using CardioEasy® Human Cardiomyocyte Digestion Solution (Cellapy), washed twice with PBS, and incubated with anti-TNNT2 antibody (Thermo Fisher, ms-295-p) conjugated with 1:200 Alexa Fluor 488 (Beyotime) for 30 min at 37 °C in the dark. After washing, they were resuspended in PBS and analyzed on an EPICS XL flow cytometer (Beckman). At least 10,000 events per sample were acquired and analyzed with FlowJo.

Western blot analysis

Cells were lysed in RIPA buffer (Thermo Fisher) containing protease and phosphatase inhibitors (Thermo Fisher). The protein concentration was determined using the BCA protein assay kit (Thermo Fisher). Equal amounts of protein (30–50 μg) were separated by SDS-PAGE (10% polyacrylamide gel) and transferred to a PVDF membrane (Millipore). The membrane was blocked with 5% non-fat milk in TBST (Tris-buffered saline with 0.1% Tween 20) for 1 h at room temperature. Incubation with the primary antibody against JPH2 (1:1000 dilution, Santa Cruz, sc-377086) was carried out overnight at 4 °C.

Table 1 Primer sequences used in experiments

Name	Forward sequence (5'-3')	Reverse sequence (5'-3')
JPH2	ACCACCACCGAGACCTACA	CCGAAGAGCCTCCAATTAACC
TNNT2	TTCACCAAAGATCTGCTCCTCGCT	TTATTACTGGTGTGGAGTGGGTGTGG
TNNI3	TTTGACCTTCGAGGCAAGTTT	CCCGGTTTTCCTTCTCGGTG
MYH6	TCTCCGACAACGCCTATCAGTAC	GTCACCTATGGCTGCAATGCT
MYH7	GGCAAGACAGTGACCGTGAAG	CGTAGCGATCCTTGAGGTTGTA
NPPA	ACAATGCCGTGTCCAACGCAGA	CTTCATTCGGCTCACTGAGCAC
NPPB	TCTGGCTGCTTTGGGAGGAAGA	CCTTGTGGAATCAGAAGCAGGTG
CAMK2D	ACACGGTGACTCCTGAAGCCAA	GTCTCCTGTCTGTGCATCATGG
GJA1	GGAGATGAGCAGTCTGCCTTTC	TGAGCCAGGTACAAGAGTGTGG
CACNA1C	CAGAGGCTACGATTTGAGGA	GCTTCACAAAGAGGTCGTGT
RYR2	AGAACTTACACACGCGACCTG	CATCTCTAACCGGACCATACTGC
ATP2A2	GATCACACCGCTGAATCTG	AGTATTGCGGGTTGTTCCAG
GAPDH	GGAGCGAGATCCCTCCAAAAT	GGCTGTTGTCATACTTCTCATGG

After washing with TBST, the membrane was incubated with a Rabbit anti-Goat IgG (H + L) Secondary Antibody (1:5000 dilution, Abcam, ab228391) for 1 h at room temperature. Protein visualization was performed using an Odyssey Infrared Imaging System (LI-COR) to detect the bound antibodies and reveal the protein bands.

Immunofluorescence staining
Cells were seeded on Matrigel-coated slide chambers and cultured for 3 days. They were then washed with PBS, fixed with 4% PFA for 10 min, permeabilized with 0.3% Triton-X for 10 min, and blocked with 1% BSA for 1 h at room temperature. For cardiomyocyte-specific marker identification, cardiomyocytes were incubated overnight at 4 °C with 1:200 rabbit monoclonal IgG α-actinin (Santa Cruz, sc-17829) and 1:200 mouse IgG1 Troponin T (Thermo Fisher, ms-295-p). For atrial and ventricular specific markers identification, cardiomyocytes were incubated overnight at 4 °C with 1:200 rabbit monoclonal IgG MYL7 (Abcam, ab205374) and 1:200 mouse IgG1κ MYL2 (Santa Cruz, sc-517244). To assess gap junction protein expression, cardiomyocytes were incubated overnight at 4 °C with 1:200 mouse monoclonal IgM connexin-43 (Cx43) (Santa Cruz, sc-59949).

After incubation, the cells were washed three times with PBS and incubated with secondary antibodies for 1 h at room temperature (1:400 Alexa Fluor 488 Goat anti-Rabbit IgG, 1:400 Alexa Fluor 594 Goat anti-Mouse IgG, Life Technology). Cell nuclei were stained with DAPI (Life Technology) for 15 min at room temperature. The samples were imaged using a Leica TCS SP8 confocal microscope (Leica).

Quantitative real-time polymerase chain reaction (qRT-PCR)
Total RNA was extracted using TRIzol reagent (Life Technology). cDNA was synthesized using PrimeScript™ RT Master Mix (Takara). Gene expression levels were measured by real-time PCR using the iCycler iQ5 (Bio-Rad) with TB Green™ Premix Ex Taq™ II (Takara) and normalized to the endogenous control gene *GAPDH*. Relative quantification was analyzed using the comparative Ct method.

Contractility assessment
The contractile function was evaluated using the CardioExcyte96 system (Nanion). Cells were seeded onto 96-well plates coated with Matrigel at a density of 5×10^4 cells per well. The plate was placed in the CardioExcyte96 system, and the contractile waveforms were recorded. Parameters were analyzed using the software provided with the system.

Calcium transient measurement
Cells were loaded with the cell-membrane-permeable calcium fluorescent probe Fluo-4, AM (5 μM, Beyotime) in Tyrode's solution for 15 min at 37 °C in the dark. Calcium transient images were captured using a Leica TCS SP8 confocal microscope with an excitation wavelength of 488 nm and an emission wavelength of 520 nm. The fluorescence intensity was recorded over time, and the parameters were analyzed using ImageJ.

Transmission electron microscopy (TEM)
Cells were fixed with 2.5% glutaraldehyde in 0.1 M cacodylate buffer (pH 7.4) for 2 h at 4 °C. After fixation, the cells were post-fixed with 1% osmium tetroxide for 1 h at room temperature. The samples were then dehydrated through a series of ethanol solutions (50%, 70%, 90%, and 100%) and embedded in epoxy resin. Ultrathin Sects. (70–90 nm) were cut using a Leica EM UC7 ultramicrotome and stained with uranyl acetate and lead citrate. The sections were examined using a JEOL JEM-1400 transmission electron microscope. The distance between the PM and the SR membrane was measured using ImageJ.

Electrophysiological analysis
Cells were seeded onto CytoView plates (Axion) coated with Matrigel at a density of 2×10^5 cells per well. After culturing for 5–7 days, the plates were placed in the Maestro Edge multi-electrode array (MEA) system. The electrical activity of the cardiomyocytes was recorded at 37 °C, 5% CO_2. The parameters were analyzed using the data analysis software provided with Axion.

Lentiviral transfection for JPH2 overexpression and mutant protein expression
The viral vectors were constructed by Yunzhou Biotechnology. The full-length wild-type JPH2 cDNA was cloned into pLVX-IRES-GFP. For the mutant JPH2 constructs (G505S and E85K), site-directed mutagenesis was carried out to introduce the specific mutations. The constructed vectors were verified by Sanger sequencing. The preparation of viruses was completed by Yunzhou Biotechnology.

Target cells were cultured until reaching 30–50% confluence. The lentivirus was thawed on ice and then diluted in the cell culture medium at the determined multiplicity of infection (MOI). The diluted lentivirus was gently added to the cells, which were then incubated at 37 °C with 5% CO_2. After 15 h, the medium was replaced with fresh medium. After 48–72 h post-transfection, the transfection efficiency was evaluated by observing the expression of green fluorescent protein (GFP) under a fluorescence microscope.

Statistical analysis

All data are presented as means ± standard errors of the means (S.E.M.). Statistical significance was evaluated using two-sided Student's *t* test for two groups. Significant differences were considered when $P < 0.05$.

Results

Construction of the JPH2-knockout human embryonic stem cell-derived cardiomyocyte-like cell model

To generate the H9 hESC line with homozygous JPH2 knockout, we employed the epiCRISPR/Cas9 gene-editing system. A single guide RNA (sgRNA) was designed to target exon 2 of *JPH2* (Fig. 1A). After puromycin screening and monoclonal isolation, clones with a 16-bp deletion mutation at the target site were successfully obtained (Fig. S1A). This base deletion led to a frameshift mutation, achieving a successful ablation of the JPH2 protein.

We differentiated the mutant clones into cardiomyocytes using a chemically defined small-molecule induction method (Fig. S1B) [33]. On the 10th day of differentiation, flow cytometry was used to assess the positive rate of the cardiomyocyte marker *TNNT2* in H9 hESC-derived cardiomyocytes (WT-CMs) and JPH2 knockout H9 hESC-derived cardiomyocytes (KO-CMs). The flow cytometry results (Fig. 1B) showed that the positivity rates of TNNT2-488 fluorescence were 86.4% in WT-CMs and 85.0% in KO-CMs. The corresponding bar graph (Fig. 1C) indicated no significant difference in cardiomyocyte differentiation efficiency between the two groups, suggesting that JPH2 knockout does not affect the cardiomyocyte differentiation ability of hESCs.

Both WT-CMs and KO-CMs differentiated into ventricular, spontaneously beating cardiomyocyte-like cells, as shown in Fig. 1D. Western blot analysis on the 15th day of differentiation confirmed the successful knockout of the JPH2 protein in KO-CMs (Fig. 1E). To determine whether JPH2 knockout influenced the ratio of cardiomyocyte subtypes during In Vitro hESC differentiation, we performed immunofluorescence staining for the ventricular-specific marker MYL2 and the atrial-specific marker MYL7 in WT-CMs and KO-CMs. The immunofluorescence images (Fig. 1F) showed no significant differences in MYL2 and MYL7 expression between the two groups, indicating that JPH2 knockout does not affect the differentiation of atrial and ventricular cardiomyocytes.

JPH2-knockout cardiomyocyte-like cells display increased volume and upregulated heart failure markers in vitro

To investigate whether JPH2-knockout cardiomyocyte-like cells manifest a cardiomyopathy phenotype In Vitro, we initially employed flow cytometry to monitor the size changes of KO-CMs over different culture days. Forward scatter, which reflects cell size, was measured. The flow cytometry results (Fig. 2A) and the corresponding

bar graph (Fig. 2B) showed that while there was no significant difference in cell volume between KO-CMs and WT-CMs on day 15 of differentiation, the volume of KO-CMs increased with culture time. By day 22 and day 30, the volume of KO-CMs was significantly larger than that of WT-CMs.

Next, we performed immunofluorescence staining of cardiomyocyte myofilaments using TNNT2 and α-actinin. The immunofluorescence images (Fig. 2C and Fig. S2A) revealed that the cell surface area of KO-CMs was notably larger than that of WT-CMs, with quantitative analysis (Fig. S2B) confirming a significant increase in cell size in KO-CMs by day 30. Moreover, the quantification of disorganized sarcomeres (Fig. 2D) showed a significantly higher frequency in KO-CMs compared to WT-CMs. An increase in cardiomyocyte volume and irregular sarcomere arrangement are recognized as key morphological features of HF myocardium [34].

To further confirm whether JPH2-knockout cardiomyocyte-like cells exhibit a HF-like phenotype, we employed qRT-PCR to measure the mRNA expression levels of common HF marker genes, including *TNNT2*, *TNNI3*, *MYH7*/*MYH6*, *NPPA* and *NPPB*, in both WT-CMs and KO-CMs on day 30 of differentiation. The results (Fig. 2E) demonstrated that the expression of these marker genes was significantly upregulated in KO-CMs compared to WT-CMs. In conclusion, these findings suggest that JPH2-deficient human cardiomyocytes display a pathological phenotype resembling HF to a certain extent In Vitro.

JPH2 knockout disrupts cardiac excitation-contraction coupling in vitro

Given that contractile dysfunction is a typical feature of cardiomyopathy and myocardial ECC is crucial for normal heart function, we comprehensively examined ECC-related phenotypes in KO-CMs, including contractile function and calcium activity.

We used the CardioExcyte96 system to detect the contractile phenotype of KO-CMs. The contractile waveforms of WT-CMs and KO-CMs are presented in Fig. 3A. The statistical analysis of the contractile parameters (Fig. 3B-E) revealed that the contractile amplitude of KO-CMs was significantly lower than that of WT-CMs. Moreover, the beating frequency of KO-CMs was decreased, and the peak to peak time, time to peak, and relaxation time were all significantly prolonged. Notably, the time to peak data of KO-CMs exhibited high heterogeneity. This implies that during contraction, different cells in KO-CMs reach their contraction peaks at different times. Such temporal asynchrony is likely to undermine the heart's overall function and coordination, potentially impairing cardiac performance.
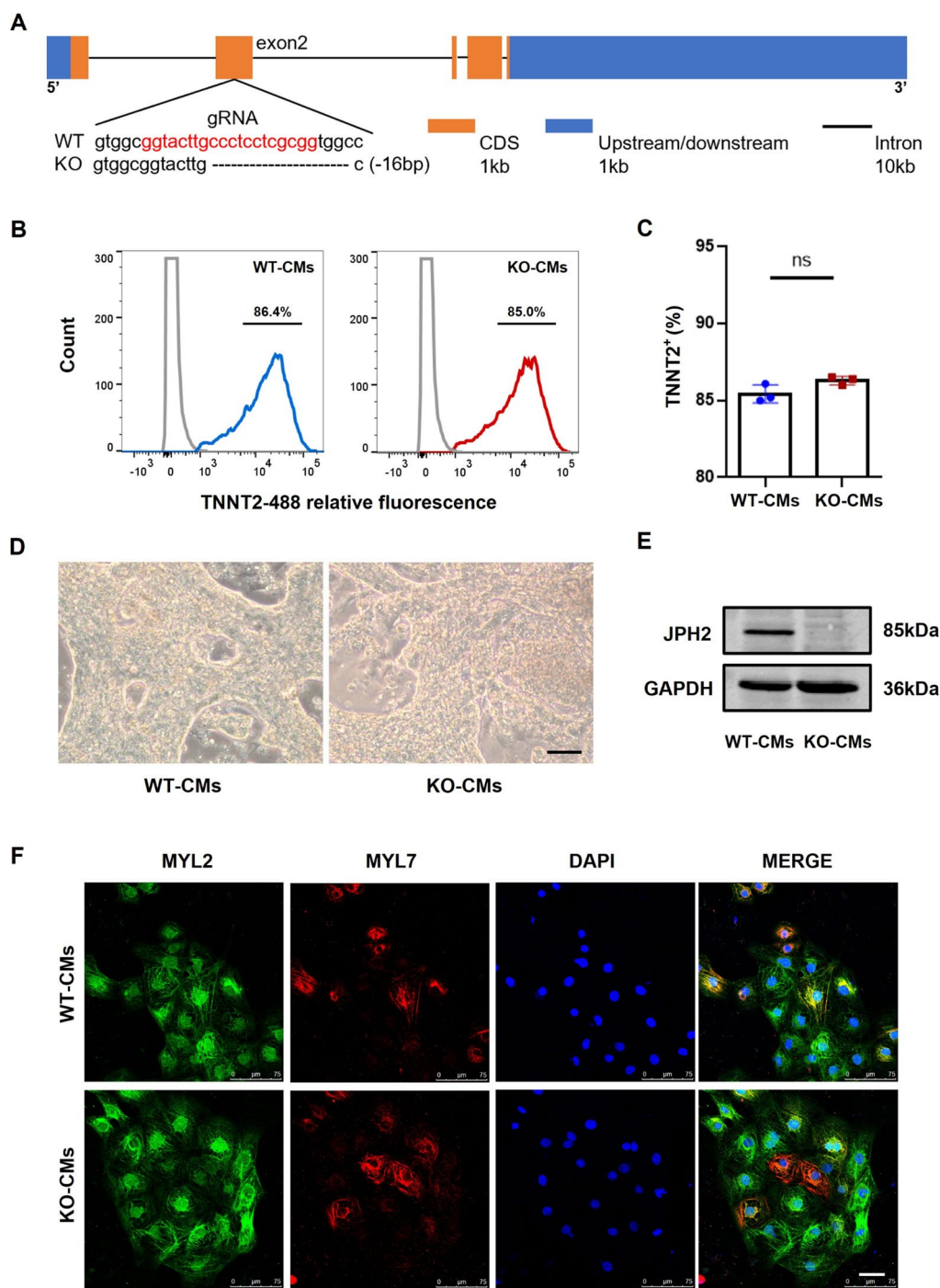
Fig. 1 Generation and characterization of JPH2-knockout hESC-derived cardiomyocytes. (**A**) Schematic of the sgRNA targeting the MORN region 2 of JPH2, resulting in a 16-bp deletion from 333 amino acids. (**B**) Flow cytometry analysis of cardiomyocyte differentiation efficiency at day 15 post-differentiation. (**C**) Bar graph showing the percentage of TNNT2-positive cells in WT-CMs and KO-CMs. (**D**) Morphology of WT-CMs and KO-CMs at day 15 post-differentiation (40x magnification). (**E**) Western blot analysis confirming the knockout of JPH2 protein in KO-CMs. Full-length blots are presented in Figure S8. (**F**) Immunofluorescence staining of ventricular-specific marker MYL2 and atrial-specific marker MYL7 in WT-CMs and KO-CMs: MYL2 in green, MYL7 in red, DAPI in blue. Scale bar = 100 μm. Results are presented as means ± SEMs of 3 independent experiments. ns, not significant, unpaired 2-sided Student's t test
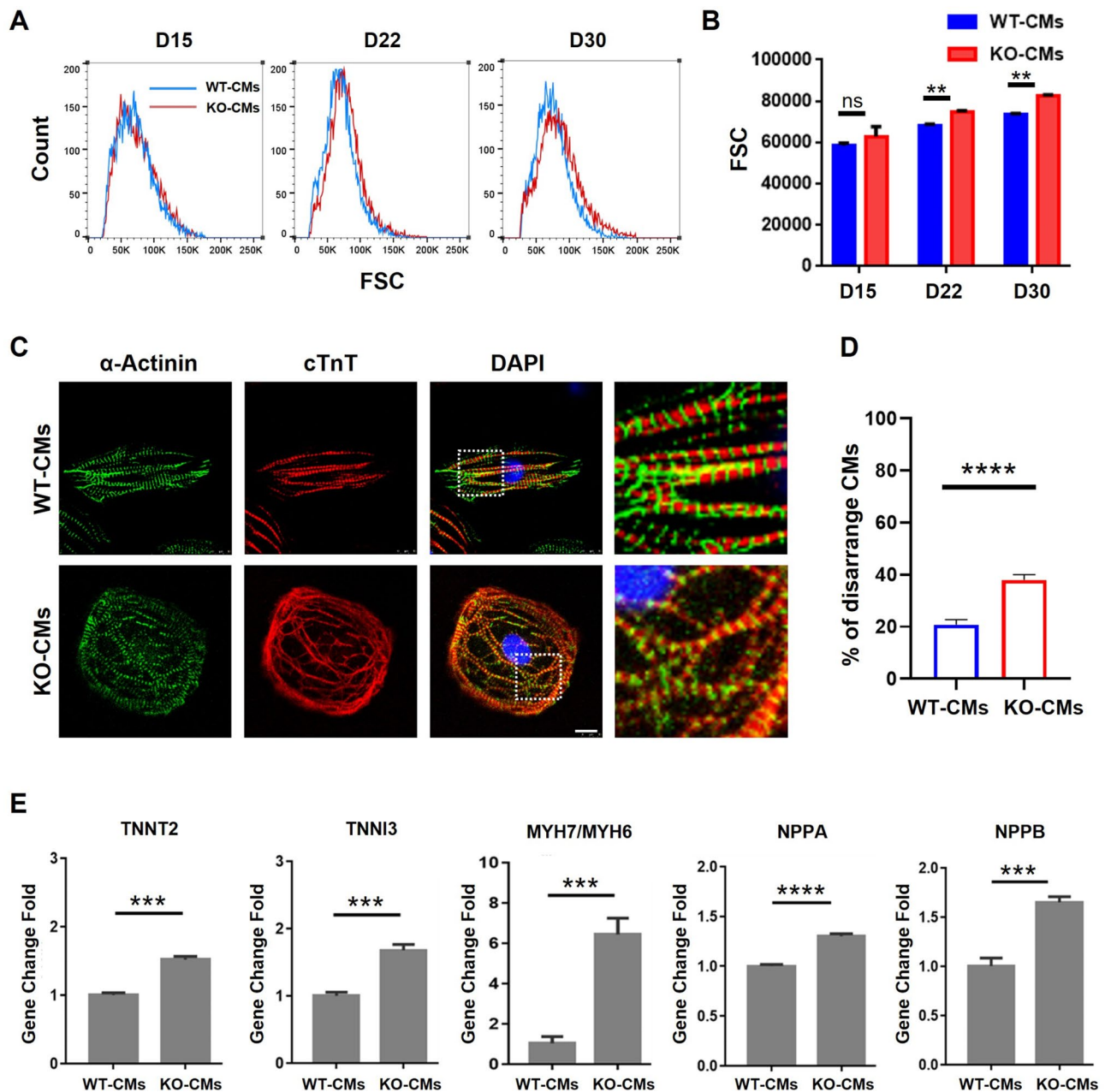
Fig. 2 JPH2-knockout cardiomyocytes exhibit hypertrophy and heart failure-like phenotypes. (**A**) Flow cytometry analysis of cell size (forward scatter) in WT-CMs and KO-CMs on Day15, 22, and 30 post-differentiation (10,000 cells/sample). (**B**) Bar graph showing the increase in cell volume of KO-CMs over time. (**C**) Immunofluorescence staining of TNNT2 and α-actinin in WT-CMs and KO-CMs at day 30 post-differentiation: α-actinin in green, cTnT in red, DAPI in blue. Scale bar = 50 μm. (**D**) Quantification of disorganized sarcomeres in WT-CMs and KO-CMs. (**E**) qRT-PCR analysis of heart failure marker genes (TNNT2, TNNI3, MYH7/MYH6, ANP, BNP) in WT-CMs and KO-CMs at day 30 post-differentiation. Results are presented as means ± S.E.M. of 3 independent experiments. ns, not significant, **$P < 0.01$; ***$P < 0.001$; ****$P < 0.0001$, unpaired two-sided Student's t test

To determine whether calcium regulation is abnormal in KO-CMs, we measured calcium transients using the cell-membrane-permeable calcium fluorescent probe Fluo-4, AM. After treating with Fluo-4, AM, we captured calcium transient images using a confocal microscope (Fig. 3F) and plotted the corresponding waveforms. The statistical analysis of calcium transient parameters (Fig. 3G-J) indicated that the calcium transient amplitude

(*F/F0*) of KO-CMs was lower than that of WT-CMs. Additionally, the calcium release time, calcium delay time, and calcium transient cycle were all significantly prolonged in KO-CMs.

Based on previous mouse model studies showing that JPH2 deficiency disrupts the JMC structure vital for cardiomyocyte ECC, we speculated a similar JMC disruption in our JPH2-knockout human cardiomyocyte model.
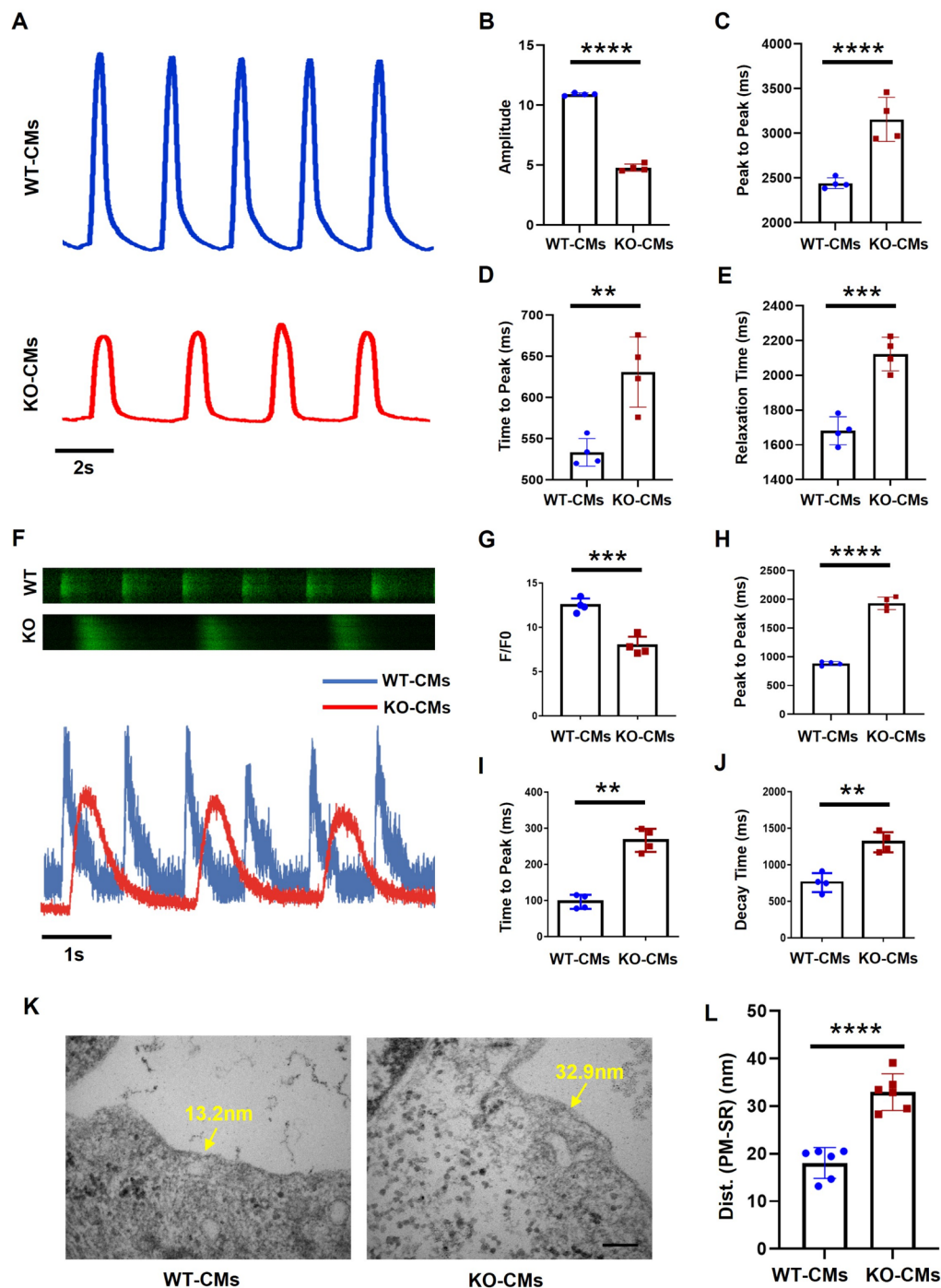
Fig. 3 JPH2 knockout disrupts excitation-contraction coupling in cardiomyocytes. (**A**) Representative contractile waveforms of WT-CMs and KO-CMs recorded by the CardioExcyte96 system at day 30 post-differentiation. (**B-E**) Statistical analysis of contractile parameters (amplitude, Peak to Peak time, Time to Peak, Relaxation Time) in WT-CMs and KO-CMs. (**F**) Representative calcium transient images and waveforms of WT-CMs and KO-CMs captured by confocal microscopy at day 30 post-differentiation. (**G-J**) Statistical analysis of calcium transient parameters (amplitude, Peak to Peak Time, Time to Peak, Delay time) in WT-CMs and KO-CMs. (**K**) Representative TEM images of the JMC structure in WT-CMs and KO-CMs at day 30 post-differentiation. Scale bar = 100 nm. (**L**) Bar graph showing the distance between the PM and SR membrane in WT-CMs and KO-CMs; *n* = 6. Results are presented as means ± S.E.M. of 4 independent experiments. **$P < 0.01$; ***$P < 0.001$; ****$P < 0.0001$, unpaired two-sided Student's t test. Abbreviations: WT, WT-CMs; KO: KO-CMs

We used TEM to examine the structure of the JMC in WT-CMs and KO-CMs (Fig. 3K). The distance between the PM and the SR membrane was measured, and the results are presented in Fig. 3L. In WT-CMs, the average distance was 18.0 ± 3.3 nm, similar to the 12–15 nm range reported in mouse models. In contrast, the average distance in KO-CMs was 32.4 ± 4.5 nm, significantly larger than that in WT-CMs. This indicates that JPH2 knockout disrupts the normal structure of the JMC in human cardiomyocytes.

In summary, in JPH2-knockout cardiomyocyte-like cells, the disruption of the JMC structure, which is pivotal for maintaining proper calcium regulation and contraction function, subsequently leads to the impairment of ECC. These alterations collectively underlie the pathological phenotype observed in these cells, offering valuable insights into the indispensable role of JPH2 in preserving normal cardiac function.

JPH2 knockout affects cardiac electrical activity and coupling delay

Having confirmed that JPH2 knockout disrupts the ECC in cardiomyocyte-like cells, we recognized the need to investigate the electrical activity underlying this process. Since electrical signals initiate and coordinate ECC, any impairment in ECC likely involves corresponding changes in electrical properties. Thus, we used an Axion MEA system to compare the electrical activity between WT-CMs and KO-CMs.

Figure 4A shows the overall electrical activity waveforms of multiple consecutive cycles, which can reflect the rhythm of cardiomyocytes. The electrical activity of KO-CMs was less regular than that of WT-CMs, indicating potential arrhythmic tendencies in JPH2-knockout cells. Analysis of the field potential duration (FPD) (Fig. 4B) demonstrated that the FPD of KO-CMs was significantly prolonged compared to that of WT-CMs. Moreover, similar to the heterogeneity observed in the time to peak during contraction, the FPD in KO-CMs also exhibited a certain degree of heterogeneity. To a certain extent, FPD can reflect the time of myocardial repolarization. The prolonged and heterogeneous FPD in KO-CMs implies abnormal repolarization processes. Since appropriate repolarization is essential for the normal refractoriness of cardiomyocytes and the accurate timing of subsequent electrical impulses, the abnormality in KO-CMs can render them more susceptible to arrhythmias, disrupting the coordinated contraction of the heart muscle and potentially compromising overall cardiac function. The action potential duration (APD) waveforms and the statistical analysis of APD90 (the time at which 90% of repolarization is achieved) are shown in Fig. 4C. Similar to the FPD results, the APD90 of KO-CMs was significantly longer than that of WT-CMs.

To further explore conduction properties and their contribution to arrhythmic potential, we assessed electrical conduction and Cx43 expression in WT-CMs and KO-CMs. Heatmaps generated from MEA recordings illustrated distinct electrical conduction patterns, with KO-CMs showing reduced conduction velocity compared to WT-CMs (Fig. S3A, B). Immunofluorescence staining at day 30 post-differentiation revealed altered Cx43 distribution in KO-CMs, suggesting impaired gap junction function (Fig. S3C). Additionally, representative field potential traces indicated that spontaneous ectopic beats were observable in KO-CMs, though their incidence remained relatively low (Fig. S3D, E), further highlighting subtle conduction abnormalities in JPH2-knockout cells.

Among the notable findings, a particularly remarkable one was the significant disparity in the ECCD, which is precisely defined as the time interval from the initiation of electrical activity to the onset of mechanical contraction (Fig. 4D). In KO-CMs, the ECCD exhibited high heterogeneity (Fig. 4E, F). This heterogeneity implies that different cells in the KO-CM population have variable time lags between electrical excitation and mechanical contraction. Such variability in ECCD can severely disrupt the synchronization of cardiac contraction, further contributing to the overall impairment of cardiac function.

In conclusion, JPH2 knockout in cardiomyocyte-like cells leads to significant abnormalities in electrical activity, including prolonged FPD and APD, reduced conduction velocity with occasional spontaneous ectopic beats, and heterogeneous ECCD. These electrical disturbances, in combination with the previously observed defects in contraction and calcium handling provide a holistically understanding of the pathological mechanisms underlying JPH2-related cardiomyopathy. The heterogeneous ECCD, in particular, may serve as a sensitive and comprehensive biomarker for assessing the severity of JPH2-associated cardiac dysfunction, as it integrates information from electrical, calcium, and mechanical aspects of cardiomyocyte function.

Wild-type JPH2 overexpression restores excitation-contraction coupling in JPH2-deficient cardiomyocytes: ECCD as a valid indicator

We have previously demonstrated that JPH2 knockout leads to significant abnormalities in cardiomyocyte contraction, calcium activity, and electrical properties. The highly heterogeneous ECCD in KO-CMs comprehensively reflects the excitation-contraction uncoupling caused by the disruption of the JMC structure. To further confirm that JPH2 deletion is the direct cause of these myocardial morphological and functional abnormalities and to explore whether overexpression of wild-type JPH2
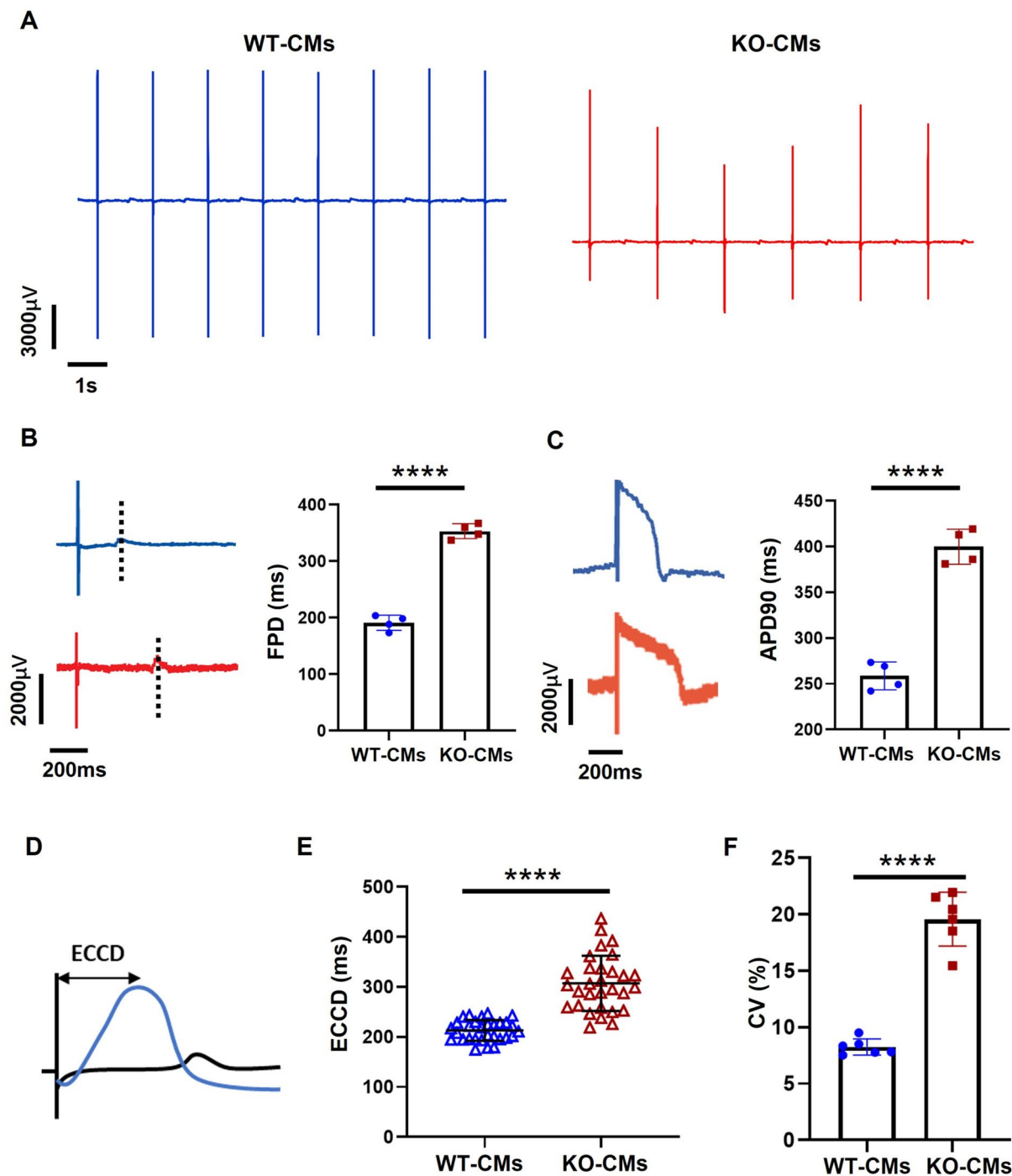
Fig. 4 JPH2 knockout leads to abnormal electrical activity and eccd heterogeneity. (**A**) Representative electrical activity waveforms of WT-CMs and KO-CMs recorded by the MEA system at day 30 post-differentiation. (**B**) Representative waveforms of electrical signal and statistical analysis of FPD in WT-CMs and KO-CMs. (**C**) Representative APD waveforms and statistical analysis of APD90 in WT-CMs and KO-CMs. (**D**) Schematic diagram of ECCD. (**E**) Scatter plot of ECCD in WT-CMs and KO-CMs. (**F**) Bar graph showing the coefficient of variation of ECCD in WT-CMs and KO-CMs; $n = 6$. Results are presented as means ± S.E.M. of 4 independent experiments. ****$P < 0.0001$, unpaired two-sided Student's t test

can ameliorate the pathological phenotypes of KO-CMs, especially the abnormal ECCD, we used lentiviral transfection to overexpress wild-type JPH2 in these cells and detected the restoration of the phenotypes (Fig. 5A).

First, to ensure the effectiveness of the overexpression vector and determine the optimal MOI, we transfected KO-CMs with different MOIs and detected the expression of GFP. As shown in Fig. S4, strong green
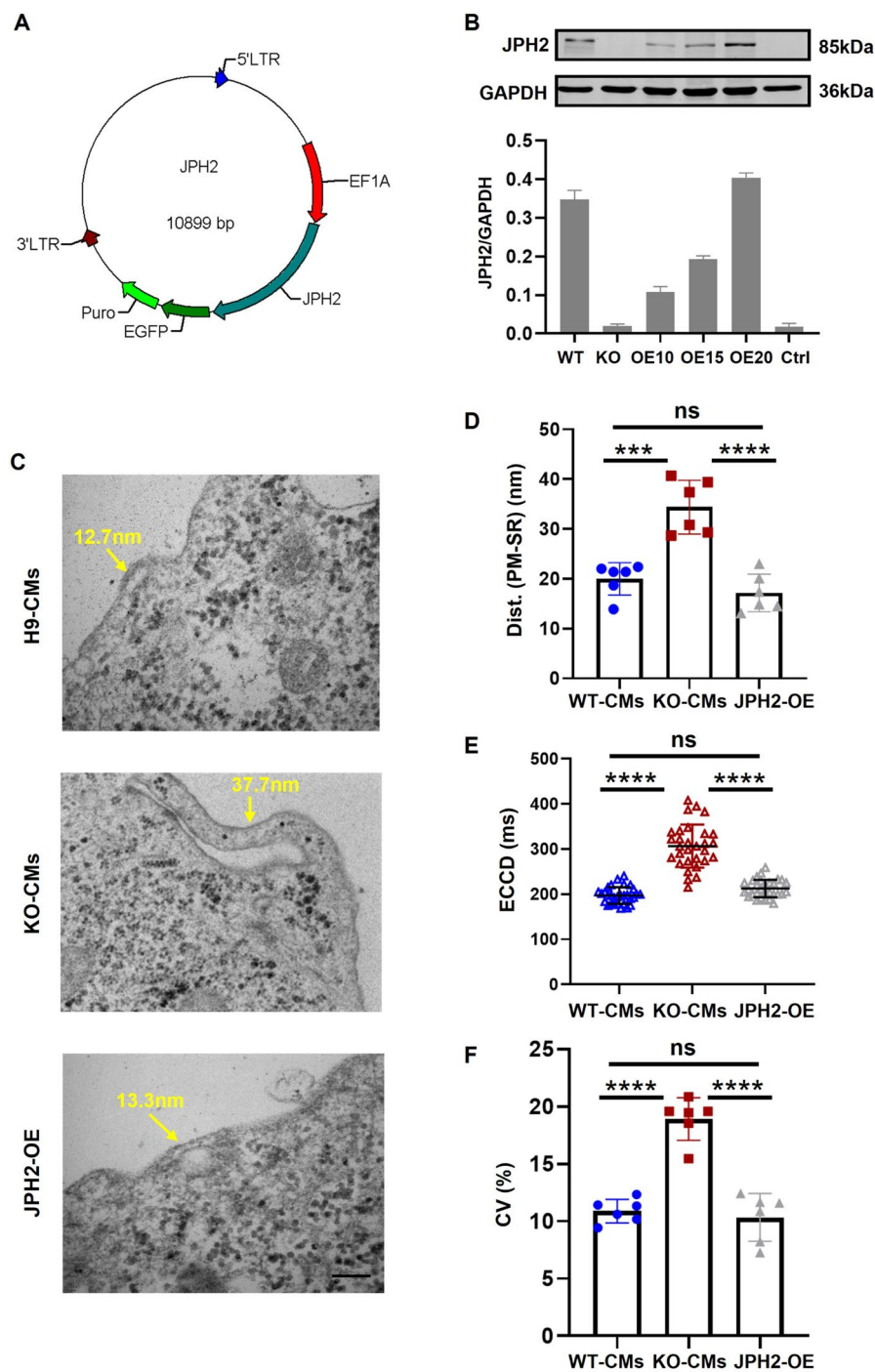
Fig. 5 Overexpression of wild-type JPH2 rescues ECC impairment in KO-CMs. (**A**) Schematic diagram of the overexpression vector backbone for lentiviral transfection. (**B**) Western blot analysis of JPH2 expression in KO-CMs transfected with different MOIs (10, 15, and 20). Full-length blots are presented in Figure S8. (**C**) Representative TEM images of the JMC structure in JPH2-OE-KO-CMs. CMs were transduced with lentivirus at two weeks post-differentiation, and phenotypes were assessed two weeks after transduction. The JMC structures are highlighted with yellow arrows. Scale bar=100nm. (**D**) Bar graph showing the distance between the PM and SR membrane in WT-CMs, KO-CMs and JPH2-OE-KO-CMs. (**E**) Scatter plot of ECCD in WT-CMs, KO-CMs and JPH2-OE-KO-CMs. To eliminate potential effects of lentiviral transfection, WT-CMs and KO-CMs were also transfected with an empty vector. (**F**) Bar graph showing the coefficient of variation of ECCD in WT-CMs, KO-CMs and JPH2-OE-KO-CMs. Results are presented as means ± S.E.M. of 6 independent experiments. ns, not significant, ***$P < 0.001$; ****$P < 0.0001$, unpaired two-sided Student's t test. Abbreviations: WT, WT-CMs; KO, KO-CMs; OE10, JPH2 overexpression at MOI=10; OE15, JPH2 overexpression at MOI=15; OE20, JPH2 overexpression at MOI=20; Ctrl, Empty vector transfection at MOI=20; JPH2-OEs, JPH2-OE-KO-CMs.

fluorescence was observed in cells when the MOI was 10, 15, and 20. We then extracted proteins from KO-CMs transfected with different MOIs and conducted Western blot analysis. The results indicated that the expression level of JPH2 protein in KO-CMs increased with the rising MOI. When the MOI was in the range of 15–20, the JPH2 expression level was comparable to that in WT-CMs (Fig. 5B). To guarantee sufficient JPH2 expression, we chose MOI = 20 to infect KO-CMs for subsequent detections.

As previously established, the loss of JPH2 disrupts the JMC structure, which is the root cause of the morphological and functional abnormalities in KO-CMs. To investigate whether restoring JPH2 expression in KO-CMs can reconstruct the JMC, we overexpressed wild-type JPH2 in KO-CMs via lentiviral transfection. TEM was used to visualize the JMC structure. As shown in Fig. 5C, distance between the PM and the SR membrane in JPH2-OE-KO-CMs (KO-CMs overexpressing wild-type JPH2) was restored to within 15 nm. The bar graph in Fig. 5D shows that the distance between the PM and the SR membrane in JPH2-OE-KO-CMs has been restored and there is no significant difference compared with that in WT-CMs. This indicates that restoring the JPH2 expression level can reconstruct the JMC in KO-CMs.

Given that the ECCD can comprehensively reflect the excitation-contraction uncoupling in KO-CMs and holds promise as a key and multi-faceted indicator for determining the disrupted coupling between electrical excitation and mechanical contraction, we further investigated whether the overexpression of wild-type JPH2 could restore the ECCD heterogeneity after reconstructing the JMC structure. We employed MEA to measure the ECCD of JPH2-OE-KO-CMs. As depicted in Fig. 5E&F, unlike the dispersed distribution of ECCD observed in KO-CMs, the ECCD of JPH2-OE-KO-CMs presented a more regular pattern. This marked improvement in the ECCD distribution provides compelling evidence that the overexpression of wild-type JPH2 can effectively rescue the ECC impairment in JPH2-knockout human cardiomyocytes.

Wild-type JPH2 overexpression restores contractile function and calcium activity in JPH2-deficient cardiomyocytes

Following the confirmation that overexpression of wild-type JPH2 can rescue the ECC impairment in JPH2-deficient cardiomyocytes as evidenced by the restoration of the ECCD, we further investigated the contractile function and calcium activity of JPH2-OE-KO-CMs to thoroughly assess the recovery of ECC and validate the feasibility of ECCD as an indicator.

The contractile function of cardiomyocytes is a direct manifestation of effective ECC. As shown in Fig.S5A-E,

the contractility detection results revealed significant improvements in JPH2-OE-KO-CMs. Specifically, the contractile amplitude of JPH2-OE-KO-CMs was notably increased compared to that of KO-CMs. Moreover, parameters such as peak to peak, time to peak, and relaxation time of JPH2-OE-KO-CMs were all restored to more normal levels due to the overexpression of JPH2.

Calcium ions play a central role in ECC, acting as the key messenger between electrical excitation and mechanical contraction. The calcium transient detection results presented in Fig. S5F-J provided further evidence of the restoration of ECC in JPH2-OE-KO-CMs. The calcium transient amplitude of JPH2-OE-KO-CMs was significantly increased compared to that of KO-CMs and was comparable to that of WT-CMs. This indicates that the ability of JPH2-OE-KO-CMs to release and handle calcium ions during each excitation-contraction cycle has been restored to a normal state. Additionally, the calcium transient duration, calcium release time, and calcium recovery time of JPH2-OE-KO-CMs were all restored to normal levels. These findings suggest that the calcium handling machinery within the cardiomyocytes, including the release from the sarcoplasmic reticulum and re-uptake processes, has been properly re-established.

The restoration of both contractile function and calcium activity in JPH2-OE-KO-CMs is consistent with the previously observed normalization of ECCD. ECCD reflects the time lag between electrical excitation and mechanical contraction, and its restoration implies a more coordinated coupling between these two processes. The concurrent recovery of contractile function and calcium activity further confirms that the normalization of ECCD is not an isolated event but a representative manifestation of the overall restoration of ECC. This provides compelling evidence for the feasibility of utilizing ECCD as a comprehensive and reliable indicator to assess both the severity of cardiac diseases caused by JPH2 pathogenic variants. In addition, these results demonstrate that overexpression of wild-type JPH2 can effectively restore ECC in JPH2-deficient myocardium, highlighting the potential of targeting JPH2 for the treatment of cardiac diseases associated with ECC impairment.

In addition, to further explore potential therapeutic strategies for restoring ECC in JPH2-deficient cardiomyocytes, we treated KO-CMs with the calcium channel agonist Bay K 8644. As shown in Fig. S6, the calcium transient amplitude, ECCD heterogeneity, and the upregulation of heart failure markers in KO-CMs were significantly improved following treatment. These results suggest that pharmacological modulation of calcium handling can partially rescue the ECC impairment and pathological phenotype caused by JPH2 deficiency, highlighting the potential of targeting calcium regulation as a therapeutic approach for JPH2-related cardiomyopathy.

Validation of ECCD as an indicator for the pathogenic severity of JPH2 mutations

Based on the findings that the ECCD can serve as a comprehensive indicator for assessing the severity of ECC impairment, we further investigated whether ECCD could accurately reflect the pathogenic severity of different JPH2 point mutations. For this purpose, we chose two JPH2 point mutations: G505S, a well-characterized benign mutation, and E85K, a mutation that has been documented in family pedigrees to induce cardiac dysfunction. These mutations were then overexpressed in KO-CMs via lentiviral vectors.

Figure 6A shows the schematic diagram of the localization of the two point mutations on the JPH2 protein. The E85K mutation is located in the MORN domain, an important domain for the binding of JPH2 to the T-tubule/PM. In contrast, the G505S mutation is situated in the variable region, a non-conserved domain. This difference in localization may underlie the distinct pathogenic effects of these two mutations. To achieve the overexpression of the mutant JPH2 proteins in KO-CMs, we used lentiviral vectors with the MOI of 20. Figure 6B presents the GFP fluorescence images after transfection. The strong GFP signals indicate efficient transfection of the lentiviral vectors carrying the mutant JPH2 constructs, suggesting that the mutant proteins were successfully introduced into the KO-CMs.

We then measured the ECCD of JPH2-OE-KO-CMs, KO-CMs, G505S mutant-CMs (G505S-CMs), and E85K mutant-CMs (E85K-CMs). The ECCD scatter plots in Fig. 6C reveal significant differences in ECCD heterogeneity among these groups. G505S-CMs showed relatively homogeneous ECCD, similar to JPH2-OE-KO-CMs. In contrast, E85K-CMs exhibited heterogeneous ECCD. The bar graph of the coefficient of variation of ECCD heterogeneity in Fig. 6D further quantifies these differences, providing evidence that ECCD can distinguish between the effects of different JPH2 mutations.

To further validate the accuracy of ECCD in reflecting the pathogenic severity, we examined the cardiac contraction of G505-CMs and E85K-CMs. Figure 6E shows the cardiac contraction waveforms, and Fig. 6F-I present the analysis of related parameters. These results are consistent with the ECCD findings. The G505S-CMs exhibited normal contraction, which was consistent with that of the JPH2-OE-KO-CMs. In contrast, the E85K-CMs with heterogeneous ECCD showed abnormal contraction characteristics, including a decrease in amplitude and an extension of the contraction cycle.

In addition, conduction velocity was reduced in KO-CMs and E85K-CMs compared to OE-CMs (Fig. S7A, B), suggesting impaired electrical propagation in these variants. qRT-PCR analysis revealed that Cx43 expression was most significantly reduced in KO-CMs and E85K-CMs compared to WT-CMs (Fig. S7C), indicating severely impaired gap junction function in these pathogenic variants. In contrast, calcium-handling gene expression showed distinct patterns across groups: KO-CMs exhibited pronounced upregulation of these genes, particularly reflecting dysregulated calcium homeostasis, while E85K-CMs displayed a notable upregulation of CACNA1C alongside moderate changes in other calcium-handling genes (Fig. S7D).

Collectively, these findings establish that ECCD heterogeneity serves as a dependable measure of the functional consequences of JPH2 mutations, with the G505S and E85K variants displaying divergent effects on cardiomyocyte contractility and excitation-contraction coupling delay profiles. These observations reinforce the robustness and value of ECCD as a holistic indicator for evaluating JPH2-associated cardiac dysfunction.

Discussion

Establishment and phenotypic characterization of the JPH2-knockout model

In this study, we established a JPH2-knockout hESC-CM model to investigate the role of JPH2 in human cardiac function and the potential mechanisms by which JPH2 down-regulation leads to related cardiac diseases. Our research outcomes not only present a comprehensive and systematic phenotypic characterization within the human-derived model for the pathophysiology of JPH2-related disorders but also offer potential indicators for accurately evaluating the severity of cardiac diseases linked to ECC impairment.

Previous investigations using animal models have offered valuable insights into JPH2's role in cardiac physiology. For instance, JPH2-knockdown mice exhibit profound cardiac dysfunction, characterized by disrupted JMC structures and impaired CICR [10, 29, 30]. These observations closely parallel our results in the hESC-CM model, where JPH2 deletion similarly induced significant JMC disruption. Furthermore, animal studies have demonstrated that JPH2 deficiency reduces calcium transient amplitude, a finding corroborated by our data showing diminished SR calcium release in knockout cells [10, 30, 35]. However, while animal models often manifest early lethality or overt heart failure, our in vitro human platform enables prolonged and controlled observation of cellular phenotypes. This approach uncovered progressive abnormalities in contraction and electrical activity, suggesting early cellular changes that may precede organ-level pathology and offering a complementary perspective to in vivo findings.

In our JPH2-knockout model, the deletion of JPH2 caused significant disruption to the JMC structure. Transmission electron microscopy revealed an increased distance between the PM and the SR membrane,
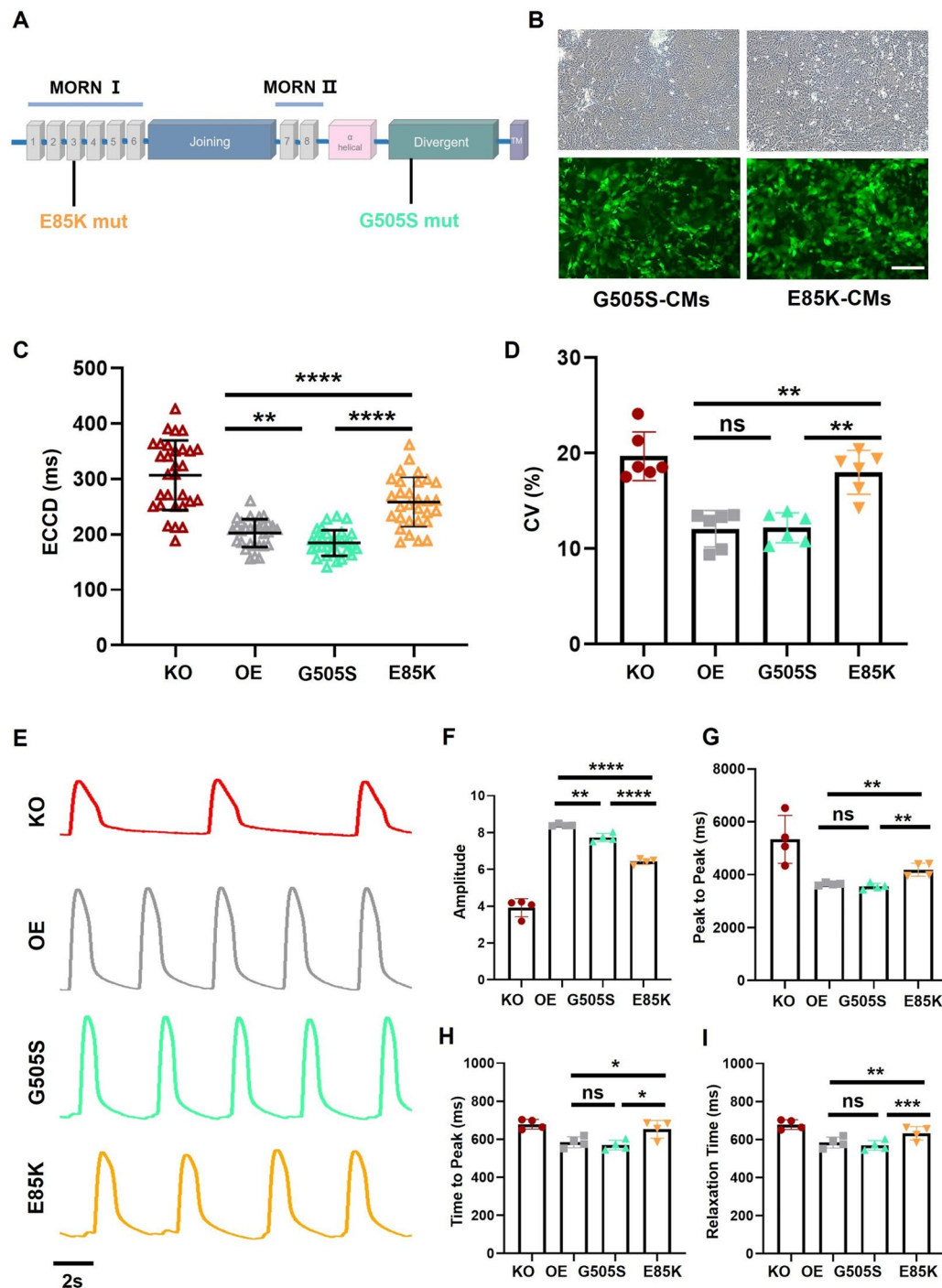
Fig. 6 ECCD as a sensitive indicator for assessing the pathogenic severity of JPH2 mutations. (**A**) Schematic diagram of the localization of G505S and E85K mutations on the JPH2 protein structure. (**B**) GFP fluorescence images of KO-CMs transfected with lentiviral vectors carrying G505S and E85K mutations. (**C**) Scatter plots of ECCD in JPH2-OE-KO-CMs, KO-CMs, G505S-CMs, and E85K-CMs. To eliminate potential effects of lentiviral transfection, KO-CMs were also transfected with an empty vector. (**D**) Bar graph showing the coefficient of variation of ECCD heterogeneity in JPH2-OE-KO-CMs, KO-CMs, G505S-CMs, and E85K-CMs; $n = 6$. (**E**) Representative contraction waveforms of KO-CMs, JPH2-OE-KO-CMs, G505S-CMs, and E85K-CMs. (**F-I**) Statistical analysis of contraction parameters, including amplitude, Peak to Peak time, Time to Peak, and Relaxation Time. Results are presented as means ± S.E.M. of 4 independent experiments. ns, not significant, $*P < 0.05$; $**P < 0.01$; $***P < 0.001$; $****P < 0.0001$, unpaired two-sided Student's t test. Abbreviations: KO, KO-CMs; OE, JPH2-OE-KO-CMs; G505S, G505S-CMs; E85K, E85K-CMs

Guo *et al. Stem Cell Research & Therapy*   (2025) 16:234

Page 15 of 18

indicating the impairment of the JMC. This structural damage had a profound impact on the ECC process in cardiomyocytes. The loss of JPH2 disrupted the JMC structure, leading to an increased distance between LTCC and RyR2. This structural impairment led to inefficient CICR and reflected in the calcium transient process [4]. There was a significant reduction in the amplitude of calcium transients, indicating a diminished ability of the SR to release calcium. Moreover, the time to peak of calcium transients was notably prolonged, suggesting a delay in the initiation and progression of calcium release. Concurrently, the contraction parameters also exhibited consistent abnormalities. The contractile amplitude of JPH2-deficient cardiomyocytes decreased significantly, and the peak to peak time, time to peak, and relaxation time were all significantly prolonged, mirroring the impairment in calcium-related processes.

The uncoupling was not only evident in calcium handling and contraction but also prominent in the electrical activity of cardiomyocytes. Analysis of the FPD and APD revealed a significant prolongation, indicating abnormal repolarization processes. This abnormal repolarization can disrupt the normal refractoriness of cardiomyocytes and the accurate timing of subsequent electrical impulses, increasing the susceptibility to arrhythmias. In conclusion, our results strongly suggest that the deletion of JPH2 comprehensively disrupts the ECC process by destroying the JMC structure. This disruption gives rise to a spectrum of abnormal phenotypes in electrical activity, calcium handling, and contractile function in JPH2-deficient human cardiomyocytes. These findings underscore the indispensable role of JPH2 in maintaining the integrity and proper functioning of ECC in cardiomyocytes. These findings, consistent with and extending animal model data, affirm JPH2's critical role in sustaining ECC integrity and functionality, while highlighting the unique advantages of a human-derived system for dissecting cellular mechanisms.

ECCD as a comprehensive indicator of ECC impairment

The ECCD is a parameter that reflects the time interval from the initiation of electrical activity to the onset of mechanical contraction. While single indicators of contraction, calcium handling, or electrical activity can reflect disruptions in the ECC to some extent, JPH2 mutations may cause damage not only by disrupting the JMC but also through other pathways, such as interacting with ion-channel proteins and acting as a stress-adaptive transcription regulator [36–42]. Therefore, a comprehensive indicator like ECCD, which encompasses electrical, calcium, and mechanical aspects, can more comprehensively and holistically reflect the pathogenicity associated with JPH2 mutations.

In our study, we found that ECCD is a highly sensitive and comprehensive indicator for assessing the severity of JPH2-related cardiac dysfunction. In JPH2-deficient cardiomyocytes, the ECCD time was significantly increased and showed a dispersed distribution, indicating a lack of synchronization between electrical excitation and mechanical contraction. This heterogeneity in ECCD is closely related to the disrupted JMC structure and abnormal calcium activity, as it reflects the inefficiency of CICR and the uncoupling of ECC. Compared to traditional indicators, ECCD integrates information from electrical, calcium, and mechanical aspects of cardiomyocyte function. It can provide a more holistic view of the ECC process and better reflect the overall cardiac function. Moreover, our results showed that ECCD can accurately distinguish between the effects of different JPH2 point mutations, further demonstrating its potential as a reliable diagnostic and prognostic marker for diseases caused by the disruption of ECC. However, its clinical utility remains to be validated in more heterogeneous human populations. Future investigations using patient-derived cardiomyocytes or in vivo models could confirm ECCD's sensitivity and specificity across diverse genetic backgrounds.

Looking ahead, the integration of computational prediction models, such as AlphaFold, with ECCD-based functional assays could further enhance our ability to assess the pathogenicity of JPH2 mutations. AlphaFold's ability to predict the structural and functional impact of point mutations, combined with the sensitivity of ECCD in reflecting ECC, may enable a more efficient and accurate approach to evaluating disease severity. While this study tested only two JPH2 variants, broader screening of additional mutations is ongoing to validate ECCD's generalizability across diverse pathogenic mechanisms. These results will be reported in subsequent publications. Such a platform could be extended to screen other mutations or proteins involved in cardiac dysfunction, offering new insights into disease mechanisms and potential therapeutic targets. Future studies could explore the development and validation of this approach, paving the way for its application in disease diagnosis and personalized medicine.

Restoration of ECC function through genetic and Pharmacological interventions

To further confirm the causal relationship between JPH2 deletion and the abnormal cardiac phenotypes, we overexpressed wild-type JPH2 in JPH2-deficient cardiomyocytes. The results showed that overexpression of JPH2 could effectively restore the JMC structure, re-establish the ECC process, and normalize the ECCD time. In addition, the contractile function and calcium activity of the cardiomyocytes were also restored to near-normal

levels. We also found that treatment with a L-type calcium channel agonist partially rescued the ECCD and calcium phenotypes, suggesting its potential role in ameliorating JPH2-related dysfunction. These findings indicate that targeting JPH2 could be a promising therapeutic strategy for HF-related cardiomyopathy. By increasing the expression of JPH2, we can potentially repair the damaged JMC structure, improve calcium regulation, and enhance the synchronization of ECC, thereby rescuing the myocardial function damage. While short-term Bay K 8644 treatment showed promising effects on calcium transients, its long-term impacts on cell survival, arrhythmogenicity, or hypertrophy remain unexplored. Future studies will investigate chronic treatment effects to assess its therapeutic viability.

Limitations and future directions

While this study yields significant insights into JPH2's role in cardiac function, certain limitations must be acknowledged to contextualize our findings and guide future efforts. The hESC-CM model, though a powerful tool for recapitulating human-specific cardiomyocyte phenotypes, falls short of fully mirroring the in vivo environment. Notably, the absence of mature T-tubules in these cells—despite the presence of functional JMC structures that support reliable ECCD measurements—may temper the translational relevance of our observations [43, 44]. Additionally, the vesicular SR morphology observed in our TEM images, resembling that of embryonic mouse cardiomyocytes, underscores this immaturity, potentially limiting JMC visualization [7, 45, 46]. As T-tubule maturation could enhance ECC precision, future studies could leverage advanced maturation techniques, such as mechanical or electrical stimulation, to align the model more closely with adult human cardiomyocytes [47–49].

Moreover, our investigation has been confined to in vitro effects of JPH2 deletion and overexpression, leaving its clinical applicability untested. Future validation in patient-derived cardiomyocytes or in vivo systems will be crucial to confirm ECCD's sensitivity and specificity across diverse genetic backgrounds. Additionally, the molecular underpinnings of JPH2's role—beyond JMC structural disruption—remain underexplored. Deeper interactions, such as JPH2-LTCC/RyR2 binding or calpain-mediated proteolysis, await elucidation through proteomics or structural biology approaches (e.g., cryo-EM), which could enrich our understanding of the ECC uncoupling observed here and in animal models.

Looking forward, ongoing efforts to screen a broader array of JPH2 variants will further test ECCD's generalizability, with results to be shared in subsequent publications. Similarly, while short-term Bay K 8644 treatment showed promise in restoring ECC function, its long-term

effects on cell survival, arrhythmogenicity, and hypertrophy remain unknown. Chronic treatment studies are underway to evaluate its therapeutic potential comprehensively. In conclusion, this study offers a holistic perspective on JPH2's critical role in ECC integrity and its disruption in cardiomyopathy, complementing animal model insights with a human-derived platform. The ECCD indicator and hESC-CM model established here provide robust tools for dissecting ECC-related diseases and assessing therapeutic strategies. Overcoming these limitations through advanced maturation, in vivo validation, and molecular analyses will be pivotal to translating these findings into clinical practice.

Conclusions

This study highlights the critical role of JPH2 in maintaining ECC through its stabilization of JMC. Deficiency in JPH2 is shown to drive cardiac dysfunction resembling heart failure, underscoring its importance in cardiac physiology. Furthermore, ECCD is established as a sensitive and comprehensive metric for evaluating the severity of JPH2-related impairments. These findings advance our understanding of JPH2 in cardiac pathology and position ECCD as a valuable tool for research and potential clinical evaluation, with JPH2 and calcium regulation emerging as promising therapeutic targets.

Abbreviations

ECC	Excitation-contraction coupling
SR	Sarcoplasmic reticulum
LTCC	L-type calcium channels
RyR2	Ryanodine receptor 2
CICR	Calcium-induced calcium release
JMC	Junctional membrane complex
JPH2	Junctophilin-2
PM	Plasma membrane
HF	Heart failure
hESC-CMs	Human embryonic pluripotent stem cell-derived cardiomyocytes
ECCD	Excitation-contraction coupling delay
gRNA	Guide RNA
Cx43	Connexin-43
TEM	Transmission electron microscopy
MEA	Multi-electrode array
MOI	Multiplicity of infection
GFP	Green fluorescent protein
sgRNA	Single guide RNA
WT-CMs	Wild-type H9 hESC-derived cardiomyocytes
KO-CMs	JPH2 knockout H9 hESC-derived cardiomyocytes
FPD	Field potential duration
APD	Action potential duration
APD90	Action potential duration at 90% repolarization
JPH2-OE-KO-CMs	KO-CMs overexpressing wild-type JPH2
G505S-CMs	G505S mutant-CMs
E85K-CMs	E85K mutant-CMs

Supplementary Information

Supplementary Material 1

Author contributions
GTW, LXJ and WFJ conceived the study and designed the experimental framework. WHY and GTW conducted the cellular experiments and performed data analysis. GTW and WHY were responsible for drafting the manuscript. ZYS and DDE carried out the cell culture experiments and were involved in data collection and assembly. YYT, ZM, and LSY contributed to the molecular experiments. ZM and MSH participated in the functional analysis. LF, QM, LXJ and LWJ assisted in revising the manuscript. MQ secured initial funding for the study and coordinated data validation efforts during revision. All authors reviewed and approved the final version of the manuscript.

Data availability
The datasets supporting the conclusions of this article are included within the article (and its additional files).

Declarations

Ethics approval and consent to participate
The H9 hESC line (WA09) used in this study was obtained from the WiCell Research Institute (Madison, WI, USA), registered with the NIH Human Embryonic Stem Cell Registry (NIH-hESC Registry Number: WAe009-A). The use of H9 hESCs complies with the National Institutes of Health (NIH) Guidelines for Human Stem Cell Research and the ethical standards outlined by the WiCell Research Institute. All experimental procedures involving H9 hESCs were conducted in accordance with the Declaration of Helsinki and the ethical guidelines for human embryonic stem cell research established by the Ministry of Science and Technology and the National Health Commission of China. No additional human subjects or embryonic materials were involved in this study.

Consent for publication
All authors have confirmed their consent for publication.

Competing interests
The authors declare that they have no conflict of interests.

Author details
[1]Fuwai Hospital, Chinese Academy of Medical Sciences and Peking Union Medical College/National Center for Cardiovascular Diseases, No. 167 Beilishi Road Xicheng District, Beijing 100037, China
[2]Beijing Laboratory for Cardiovascular Precision Medicine, The Key Laboratory of Biomedical Engineering for Cardiovascular Disease Research, Ministry of Education, Beijing Anzhen Hospital, Capital Medical University, Beijing 100029, China
[3]State Key Laboratory of Cardiovascular Disease, Key Laboratory of Pluripotent Stem Cells in Cardiac Repair and Regeneration, Fuwai Hospital, National Center for Cardiovascular Diseases, Chinese Academy of Medical Sciences and Peking Union Medical College, No. 167 Beilishi Road, Xicheng District, Beijing 100037, China
[4]College of Pulmonary and Critical Care Medicine, Chinese PLA General Hospital, Beijing 100091, China
[5]Department of Cardiology, Chinese PLA General Hospital, Beijing 100853, China
[6] State Key Laboratory of Cardiovascular Diseases and Medical Innovation Center, Shanghai East Hospital, School of Medicine, Tongji University, Shanghai 200120, China
[7]Fuwai Hospital Chinese Academy of Medical Sciences, Shenzhen, Shenzhen Key Laboratory of Cardiovascular Disease, State Key Laboratory of Cardiovascular Disease, Key Laboratory of Pluripotent Stem Cells in Cardiac Repair and Regeneration, Chinese Academy of Medical Sciences and Peking Union Medical College, Shenzhen, China
[8]National Health Commission Key Laboratory of Cardiovascular Regenerative Medicine, Fuwai Central-China Hospital, Central-China Branch of National Center for Cardiovascular Diseases, Zhengzhou, China
[9]State Key Laboratory of Cardiovascular Disease, Fuwai Hospital Chinese Academy of Medical Sciences, No. 12 Langshan Road, Nanshan District, Shenzhen, Guangdong Province 518057, China

References
1. Gaziano TA. Economic burden and the cost-effectiveness of treatment of cardiovascular diseases in Africa. Heart. 2008;94:140–4.
2. Mensah GA. Descriptive epidemiology of cardiovascular risk factors and diabetes in sub-Saharan Africa. Prog Cardiovasc Dis. 2013;56:240–50.
3. Lozano R, Naghavi M, Foreman K, Lim S, Shibuya K, Aboyans V, et al. Global and regional mortality from 235 causes of death for 20 age groups in 1990 and 2010: a systematic analysis for the global burden of disease study 2010. Lancet. 2012;380:2095–128.
4. Eisner DA, Caldwell JL, Kistamás K, Trafford AW. Calcium and Excitation-Contraction coupling in the heart. Circ Res. 2017;121:181–95.
5. Bers DM. Cardiac excitation-contraction coupling. Nature. 2002;415:198–205.
6. Gilligan DM, Bennett V. The junctional complex of the membrane skeleton. Semin Hematol. 1993;30:74–83.
7. Takeshima H, Komazaki S, Nishi M, Iino M, Kangawa K. Junctophilins: a novel family of junctional membrane complex proteins. Mol Cell. 2000;6:11–22.
8. Beavers DL, Landstrom AP, Chiang DY, Wehrens XHT. Emerging roles of junctophilin-2 in the heart and implications for cardiac diseases. Cardiovasc Res. 2014;103:198–205.
9. Zhang C, Chen B, Guo A, Zhu Y, Miller JD, Gao S, et al. Microtubule-mediated defects in junctophilin-2 trafficking contribute to myocyte transverse-tubule remodeling and Ca2 + handling dysfunction in heart failure. Circulation. 2014;129:1742–50.
10. van Oort RJ, Garbino A, Wang W, Dixit SS, Landstrom AP, Gaur N, et al. Disrupted junctional membrane complexes and hyperactive Ryanodine receptors after acute Junctophilin knockdown in mice. Circulation. 2011;123:979–88.
11. Hall DD, Takeshima H, Song L-S, Structure. Function, and regulation of the Junctophilin family. Annu Rev Physiol. 2024;86:123–47.
12. Garbino A, van Oort RJ, Dixit SS, Landstrom AP, Ackerman MJ, Wehrens XHT. Molecular evolution of the Junctophilin gene family. Physiol Genomics. 2009;37:175–86.
13. Landstrom AP, Beavers DL, Wehrens XHT. The Junctophilin family of proteins: from bench to bedside. Trends Mol Med. 2014;20:353–62.
14. Sheard TMD, Hurley ME, Smith AJ, Colyer J, White E, Jayasinghe I. Three-dimensional visualization of the cardiac Ryanodine receptor clusters and the molecular-scale fraying of dyads. Philos Trans R Soc Lond B Biol Sci. 2022;377:20210316.
15. Zhou J, Liu H, Lin Y, Zhao J. Membrane occupation and recognition nexus (MORN) motif controls protein localization and function. FEBS Lett. 2022;596:1839–50.
16. Jayasinghe I, Baddeley D, Kong CHT, Wehrens XHT, Cannell MB, Soeller C. Nanoscale organization of junctophilin-2 and Ryanodine receptors within peripheral couplings of rat ventricular cardiomyocytes. Biophys J. 2012;102:L19–21.
17. Munro ML, Jayasinghe I, Wang Q, Quick A, Wang W, Baddeley D, et al. Junctophilin-2 in the nanoscale organisation and functional signalling of Ryanodine receptor clusters in cardiomyocytes. J Cell Sci. 2016;129:4388–98.
18. Hill JA, Diwan A. Ca(2+) leak in atrial fibrillation: junctophilin-2 stabilizes Ryanodine receptor. J Am Coll Cardiol. 2013;62:2020–2.

19. Jiang M, Zhang M, Howren M, Wang Y, Tan A, Balijepalli RC, et al. JPH-2 interacts with Cai-handling proteins and ion channels in dyads: contribution to premature ventricular contraction-induced cardiomyopathy. Heart Rhythm. 2016;13:743–52.

20. Beavers DL, Wang W, Ather S, Voigt N, Garbino A, Dixit SS, et al. Mutation E169K in junctophilin-2 causes atrial fibrillation due to impaired RyR2 stabilization. J Am Coll Cardiol. 2013;62:2010–9.

21. Parikh SS, Blackwell DJ, Gomez-Hurtado N, Frisk M, Wang L, Kim K, et al. Thyroid and glucocorticoid hormones promote functional T-Tubule development in Human-Induced pluripotent stem Cell-Derived cardiomyocytes. Circ Res. 2017;121:1323–30.

22. Woo JS, Hwang J-H, Ko J-K, Weisleder N, Kim DH, Ma J, et al. S165F mutation of Junctophilin 2 affects Ca2 + signalling in skeletal muscle. Biochem J. 2010;427:125–34.

23. Matsushita Y, Furukawa T, Kasanuki H, Nishibatake M, Kurihara Y, Ikeda A, et al. Mutation of Junctophilin type 2 associated with hypertrophic cardiomyopathy. J Hum Genet. 2007;52:543–8.

24. Landstrom AP, Weisleder N, Batalden KB, Bos JM, Tester DJ, Ommen SR, et al. Mutations in JPH2-encoded junctophilin-2 associated with hypertrophic cardiomyopathy in humans. J Mol Cell Cardiol. 2007;42:1026–35.

25. Quick AP, Landstrom AP, Wang Q, Beavers DL, Reynolds JO, Barreto-Torres G, et al. Novel junctophilin-2 mutation A405S is associated with basal septal hypertrophy and diastolic dysfunction. JACC Basic Transl Sci. 2017;2:56–67.

26. Parker LE, Kramer RJ, Kaplan S, Landstrom AP. One gene, two modes of inheritance, four diseases: A systematic review of the cardiac manifestation of pathogenic variants in JPH2-encoded junctophilin-2. Trends Cardiovasc Med. 2023;33:1–10.

27. Wei S, Guo A, Chen B, Kutschke W, Xie Y-P, Zimmerman K, et al. T-tubule remodeling during transition from hypertrophy to heart failure. Circ Res. 2010;107:520–31.

28. Guo Y, VanDusen NJ, Zhang L, Gu W, Sethi I, Guatimosim S, et al. Analysis of cardiac myocyte maturation using CASAAV, a platform for rapid dissection of cardiac myocyte gene function in vivo. Circ Res. 2017;120:1874–88.

29. Reynolds JO, Chiang DY, Wang W, Beavers DL, Dixit SS, Skapura DG, et al. Junctophilin-2 is necessary for T-tubule maturation during mouse heart development. Cardiovasc Res. 2013;100:44–53.

30. Chen B, Guo A, Zhang C, Chen R, Zhu Y, Hong J, et al. Critical roles of junctophilin-2 in T-tubule and excitation-contraction coupling maturation during postnatal development. Cardiovasc Res. 2013;100:54–62.

31. Raniga K, Nasir A, Vo NTN, Vaidyanathan R, Dickerson S, Hilcove S, et al. Strengthening cardiac therapy pipelines using human pluripotent stem cell-derived cardiomyocytes. Cell Stem Cell. 2024;31:292–311.

32. Floy ME, Shabnam F, Simmons AD, Bhute VJ, Jin G, Friedrich WA, et al. Advances in manufacturing cardiomyocytes from human pluripotent stem cells. Annu Rev Chem Biomol Eng. 2022;13:255–78.

33. Burridge PW, Matsa E, Shukla P, Lin ZC, Churko JM, Ebert AD, et al. Chemically defined generation of human cardiomyocytes. Nat Methods. 2014;11:855–60.

34. Harvey PA, Leinwand LA. The cell biology of disease: cellular mechanisms of cardiomyopathy. J Cell Biol. 2011;194:355–65.

35. Landstrom AP, Kellen CA, Dixit SS, van Oort RJ, Garbino A, Weisleder N, et al. Junctophilin-2 expression Silencing causes cardiocyte hypertrophy and abnormal intracellular calcium-handling. Circ Heart Fail. 2011;4:214–23.

36. Poulet C, Sanchez-Alonso J, Swiatlowska P, Mouy F, Lucarelli C, Alvarez-Laviada A, et al. Junctophilin-2 tethers T-tubules and recruits functional L-type calcium channels to lipid rafts in adult cardiomyocytes. Cardiovasc Res. 2021;117:149–61.

37. Gross P, Johnson J, Romero CM, Eaton DM, Poulet C, Sanchez-Alonso J, et al. Interaction of the joining region in Junctophilin-2 with the L-Type Ca2 + Channel is pivotal for cardiac dyad assembly and intracellular Ca2 + Dynamics. Circ Res. 2021;128:92–114.

38. Wang W, Landstrom AP, Wang Q, Munro ML, Beavers D, Ackerman MJ, et al. Reduced junctional Na+/Ca2+-exchanger activity contributes to sarcoplasmic reticulum Ca2 + leak in junctophilin-2-deficient mice. Am J Physiol Heart Circ Physiol. 2014;307:H1317–1326.

39. Valtonen J, Prajapati C, Cherian RM, Vanninen S, Ojala M, Leivo K, et al. The Junctophilin-2 mutation p.(Thr161Lys) is associated with hypertrophic cardiomyopathy using Patient-Specific iPS cardiomyocytes and demonstrates prolonged action potential and increased arrhythmogenicity. Biomedicines. 2023;11:1558.

40. Lahiri SK, Lu J, Aguilar-Sanchez Y, Li H, Moreira LM, Hulsurkar MM, et al. Targeting calpain-2-mediated junctophilin-2 cleavage delays heart failure progression following myocardial infarction. J Mol Cell Cardiol. 2024;194:85–95.

41. Wang J, Chen B, Shi Q, Ciampa G, Zhao W, Zhang G, et al. Preventing Site-Specific Calpain proteolysis of Junctophilin-2 protects against Stress-Induced Excitation-Contraction uncoupling and heart failure development. Circulation. 2025;151:171–87.

42. Guo A, Wang Y, Chen B, Wang Y, Yuan J, Zhang L, et al. E-C coupling structural protein junctophilin-2 encodes a stress-adaptive transcription regulator. Science. 2018;362:eaan3303.

43. Karakikes I, Ameen M, Termglinchan V, Wu JC. Human induced pluripotent stem cell-derived cardiomyocytes: insights into molecular, cellular, and functional phenotypes. Circ Res. 2015;117:80–8.

44. Ribeiro MC, Tertoolen LG, Guadix JA, Bellin M, Kosmidis G, D'Aniello C, et al. Functional maturation of human pluripotent stem cell derived cardiomyocytes in vitro–correlation between contraction force and electrophysiology. Biomaterials. 2015;51:138–50.

45. Dolnikov K, Shilkrut M, Zeevi-Levin N, Danon A, Gerecht-Nir S, Itskovitz-Eldor J, et al. Functional properties of human embryonic stem cell-derived cardiomyocytes. Ann N Y Acad Sci. 2005;1047:66–75.

46. Dolnikov K, Shilkrut M, Zeevi-Levin N, Gerecht-Nir S, Amit M, Danon A, et al. Functional properties of human embryonic stem cell-derived cardiomyocytes: intracellular Ca2 + handling and the role of sarcoplasmic reticulum in the contraction. Stem Cells. 2006;24:236–45.

47. Ahmed RE, Anzai T, Chanthra N, Uosaki H. A brief review of current maturation methods for human induced pluripotent stem Cells-Derived cardiomyocytes. Front Cell Dev Biol. 2020;8:178.

48. Jun S, Song M-H, Choi S-C, Noh J-M, Kim KS, Park JH, et al. FGF4 and ascorbic acid enhance the maturation of induced cardiomyocytes by activating JAK2-STAT3 signaling. Exp Mol Med. 2024;56:2231–45.

49. Knight WE, Cao Y, Lin Y-H, Chi C, Bai B, Sparagna GC, et al. Maturation of pluripotent stem Cell-Derived cardiomyocytes enables modeling of human hypertrophic cardiomyopathy. Stem Cell Rep. 2021;16:519–33.

Publisher's note